Exploring the Mechanism of Binding of UDP-Galactopyranose to UDP-Galactopyranose Mutase by STD-NMR Spectroscopy and Molecular Modeling†

Yue Yuan,‡,§ Xin Wen,‡,§ David A. R. Sanders,|| and B. Mario Pinto*,‡

Department of Chemistry, Simon Fraser University, Burnaby, British Columbia, Canada V5A 1S6, and Department of Chemistry, University of Saskatchewan, 110 Science Place, Saskatoon, Saskatchewan, Canada S7N 5C9

Received July 12, 2005; Revised Manuscript Received August 31, 2005

ABSTRACT: UDP-galactopyranose mutase (UGM) is the key enzyme involved in the biosynthesis of Gal*f*. In this study, reliable structural binding modes of the natural substrate, UDP-Gal*p*, and inhibitor, UDP, in the UGM active site were provided with the combined use of STD-NMR spectroscopy, molecular modeling, and CORCEMA-ST calculations. UDP-Gal*p* and UDP exhibited similar binding epitopes recognized by UGM. However, the relative binding affinities of the ligands changed dramatically upon reduction of UGM, as explored by competitive STD-NMR experiments. UDP-Gal*p* competes with UDP for binding to UGM, especially when UGM is in its reduced state. Docking studies for predicting the binding mode within the active site of the two monomers in UGM explored the possibility that the mobile loop might act as a gateway for substrate binding, and the structure of the binding cleft in monomer A might be a closer approximation of the substrate-bound active site than monomer B. Important information regarding the critical interactions of UGM with UDP-Gal*p* has been obtained.

D-Galactofuranose (Gal*f*)[1] residues are found as components of the cell walls of fungi (*1*) and mycobacteria such as *Mycobacterium tuberculosis* and *Mycobacterium leprae* (*1*), and in cell-surface structures of protozoa such as *Trypanosoma cruzi* and *Leishmania* species (*2*−*4*). Significantly, Gal*f* is absent in mammalian glycoconjugates (*3*), and its presence in cell-surface structures appears to be essential for the survival and infectivity of microorganisms. Hence, the enzymes involved in both the formation and incorporation of Gal*f* in bacteria and parasites have become important drug targets.

UDP-galactofuranose (UDP-Gal*f*) is known to be the activated precursor for the construction of Gal*f*-containing oligosaccharides, and is synthesized from UDP-galactopyranose (UDP-Gal*p*) in a reaction catalyzed by UDP-galactopyranose mutase (UGM) (*5*, *6*). Gal*f* is then transferred onto acceptors to form various glycoconjugates by galactofuranosyltransferase. UGM is critical for the viability of *Mycobacterium smegmatis*, a model organism for *M. tuberculosis* (*7*). Therefore, the inhibition of either the interconversion of Gal*p* to Gal*f* or the transfer of the Gal*f* residue (galactosylation) is a promising strategy for the development of new therapeutic agents. Consequently, knowledge of the ligand binding properties of the enzymes, particularly the exact ligand topographies or epitopes that are recognized, is critical for the design of such inhibitors, and will also yield insights into the mechanistic aspects of Gal*f* biosynthesis.

The first crystal structure of UGM from *Escherichia coli* EC 5.4.99.9 has been determined at 2.4 Å resolution (*8*). The novel structure shows that the flavin nucleotide is located in domain 1 with the *re* face of the isoalloxazine ring open to a cleft lined with conserved residues. Site-directed mutagenesis studies indicate that this cleft contains the active site; the sugar ring of the substrate UDP-Gal*p* **1** is presumably located adjacent to the exposed isoalloxazine ring of FAD. It has also been established that the enzyme is active only when the flavin is reduced (Scheme 1) (*8*). Recently, the structures of UGM from *M. tuberculosis* and *Klebsiella pneumoniae* with FAD have been determined at 2.25 and 2.2 Å resolution, respectively (*9*). The first structure of UGM in the (active) reduced state has also been obtained for *K. pneumoniae* at 2.35 Å resolution (*9*). The structures of all four UGMs are essentially identical, with the only differences occurring in the positioning of a mobile loop located next to the active site (*9*). However, attempts to obtain the crystal structure of the complex of UDP-Gal*p* **1** and UGM have been unsuccessful. The binding mode of UDP-Gal*p* **1** in the active site of UGM and the mechanism of UGM are not yet completely resolved, and are still the subject of active investigation (*8*−*11*).

† This work was supported by Discovery Grants administered by the Natural Sciences and Engineering Research Council of Canada to both B.M.P. and D.A.R.S.

* To whom correspondence should be addressed: Department of Chemistry, Simon Fraser University, Burnaby, British Columbia, Canada V5A 1S6. Telephone: (604) 291-4152. Fax: (604) 291-4860. E-mail: bpinto@sfu.ca.

‡ Simon Fraser University.

§ These authors contributed equally to this work.

|| University of Saskatchewan.

[1] Abbreviations: Gal*f*, galactofuranose; Gal*p*, galactopyranose; UMP, uridine 5′-monophosphate; UDP-Gal*f*, UDP-D-galactofuranose; UDP-Gal*p*, UDP-D-galactopyranose; UGM, uridine 5′-diphosphate 1-galactopyranose mutase; FAD, flavin adenine dinucleotide; NMR, nuclear magnetic resonance; STD, saturation transfer difference; TOCSY, total correlation spectroscopy; CORCEMA-ST, complete relaxation and conformational exchange matrix analysis of saturation transfer; rmsd, root-mean-square deviation.

10.1021/bi0513406 CCC: $30.25
Published on Web 10/06/2005

Scheme 1

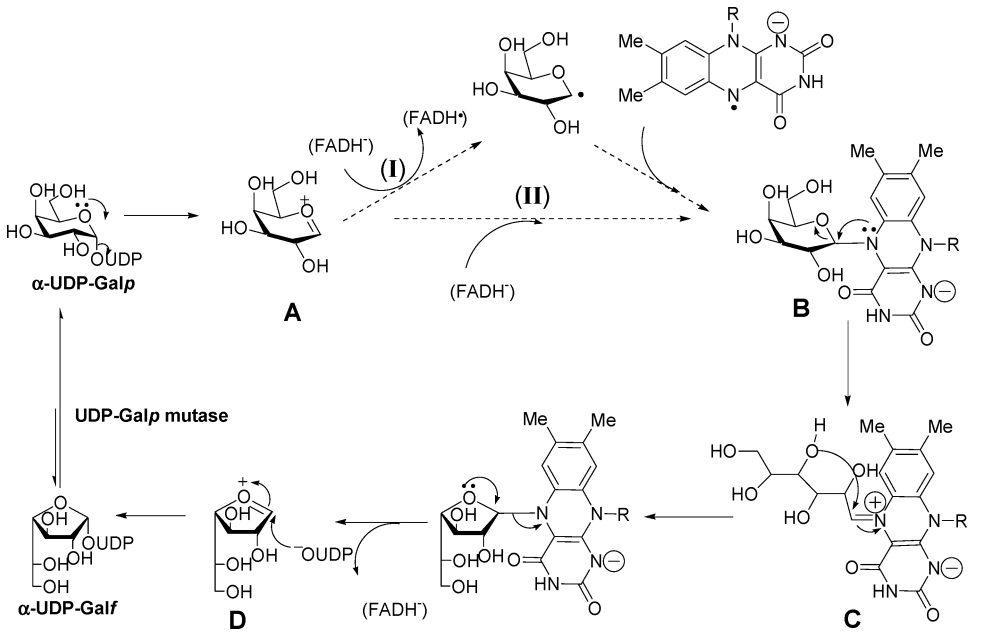

Chart 1

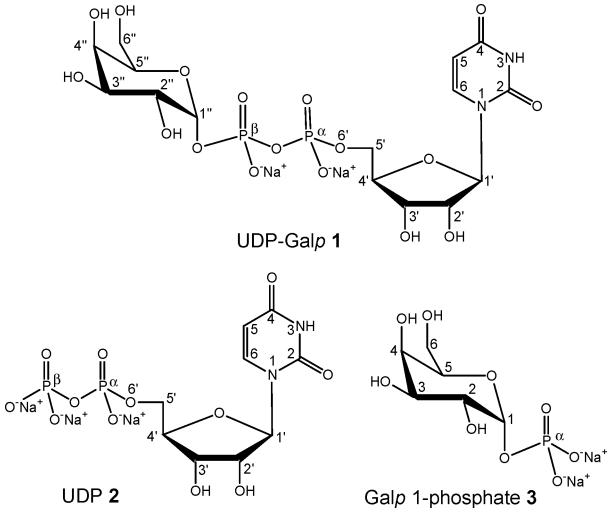

STD-NMR spectroscopy has proven to be effective in the study of binding of ligand to protein (*12*). A dramatic advance in epitope mapping was provided recently by use of simulated annealing refinement together with the CORCEMA-ST program (*13*, *14*) to derive bound conformations of ligands in the receptor protein (*15*). We have recently validated a protocol that combines STD-NMR effects with AutoDock 3.0 (*16*) calculations and the calculation of saturation effects using the CORCEMA-ST program (*13*) to predict the binding modes of glycosidase inhibitors to Golgi α-mannosidase II (*17*). Excellent correlation between calculated structures and those obtained by X-ray crystallography was obtained. We report herein the STD-NMR study of the complex of UDP-Gal*p* **1**, UDP **2**, and galactopyranose 1-phosphate (Gal*p* 1-phosphate) **3** (Chart 1) with UGM in both oxidized and reduced states. The epitopes of UDP-Gal*p* **1** and UDP **2** bound to UGM have been mapped. NMR titration experiments have shown that UDP-Gal*p* **1** competes with UDP **2** for binding to UGM, especially when UGM is in its reduced state. UDP-Gal*p* **1**, UDP **2**, and Gal*p* 1-phosphate **3** were then docked into the putative active site within monomer A and monomer B of UGM, obtained from the X-ray crystal structure (*8*), using AutoDock 3.0 (*16*). On the basis of the resulting complexes, theoretical STD effects for the ligand protons were calculated using the CORCEMA-ST program (*13*). The predicted STD values for UDP-Gal*p* **1** and UDP **2** docked in monomer A compared favorably with the experimental values, thus lending credence to the binding model. Different results shown in the docking study for monomer B allowed us to explore the role of the flexible loop in UGM for substrate binding.

EXPERIMENTAL PROCEDURES

NMR Spectroscopy. The NMR samples were prepared according to our previously published method (*8*, *18*). To a sample of UGM (1.0 mg) in phosphate-buffered saline solution [50 mM K_2HPO_4/KH_2PO_4 and 99% D_2O (pH 7.6)] was added either UDP-Gal*p* **1** (1.56 mg) or UDP **2** (1.31 mg). The final ligand concentration was 4 mM at a ligand:protein ratio of 100:1. The ligand resonances were assigned using $^1H-^1H$ TOCSY and $^1H-^{13}C$ HMQC NMR spectroscopy. The sample of reduced UGM was made by adding a freshly prepared sodium dithionite solution to the NMR sample under an atmosphere of N_2 (*8*, *18*).

The STD-NMR spectra were recorded on a Bruker AMX-600 NMR spectrometer at 285 K, as described in previous publications (*19*, *20*). The STD-NMR spectra were recorded with 1024 scans and selective saturation of protein resonances at −1.0 ppm (30 ppm for reference spectra) using a series of 40 Gaussian-shaped pulses (50 ms, 1 ms delay between pulses, $\gamma B_1/2\pi = 110$ Hz), for a total saturation time of 2.04 s. The protein resonances are broad and have significant intensity in the region downfield from 10 ppm and even at negative parts per million values (*19*, *20*). Thus, irradiation of −1.0 ppm is expected to result in saturation of protein resonances, from the aliphatic to the aromatic. Irradiation at −1.0 ppm was also considered prudent in achieving selective saturation of the protein resonances since a ligand resonance was present at 8.0 ppm. Subtraction of saturated spectra from reference spectra was performed by phase cycling (*19*, *20*).

Measurement of enhancement intensities was performed by direct comparison of STD-NMR spectra and reference one-dimensional ^{1}H NMR spectra. Data processing was performed using XWINNMR (Bruker). Reference experiments using the free ligands themselves were performed under the same experimental conditions to verify true ligand binding. No signal was present in the difference spectra, indicating that the effects observed in the presence of the protein were due to true saturation transfer.

Molecular Modeling. The molecular structures of UDP-Gal*p* **1**, UDP **2**, and Gal*p* 1-phosphate **3** for docking studies were constructed with Sybyl 6.6 (Tripos, Inc.). The five-membered ring moiety of **1** and **2** was used in a $_3$E conformation; the galactopyranose moiety of **1** and **3** was used in a $^4C_1$ chair conformation. The structure energy minimization was performed using the standard Tripos molecular mechanics force field (*21*) and Gasteiger−Marsili charges (*22*, *23*), with a 0.001 kcal/mol energy gradient convergence criterion. The atom charges were retained on **1**−**3** for the docking calculations.

The 2.4 Å resolution crystal structure of UGM (PDB entry 1I8T) (*8*) was used as the model for the macromolecule in docking studies of **1**−**3**. The model was prepared using Sybyl 6.6 (Tripos, Inc.). The water was removed. Only polar hydrogens were added to the protein, and Kollman united-atom partial charges (*24*) were assigned.

First, **2** and **3** were docked into the active site of UGM using AutoDock 3.0 (*16*). In these cases, the initial structures of **2** and **3** were manually positioned within the putative active site of UGM. Atomic affinity grid maps were computed for each atom type in compounds **2** and **3**, as well as an electrostatic grid map using AutoGrid 3.0 (*16*). The grid maps were constructed using 60 × 60 × 60 points, with grid point spacing of 0.375 Å, and centered on the ligand. A Lamarckian Genetic Algorithm (LGA) was used to search each conformation space for low-energy binding orientations. The default setting was adopted, and 300 LGA docking runs were performed.

Subsequently, **1** was docked into the putative active site of UGM. The UGM−**2** and UGM−**3** complex structures from the docking experiments described above served as starting points for building an initial structure of **1**. This was accomplished by linking the terminal P atom of UDP **2** with the anomeric O1 atom of **3** bound in UGM. Then, the torsion angles between the uridine and galactopyranose moieties of **1** were energy minimized to achieve a reasonable structure. These procedures in effect placed a reasonable starting structure of **1** within the active site of UGM. All 15 active torsions of **1** were selected to be fully flexible during the docking experiment with AutoDock 3.0 (*16*). The grid maps were constructed using 70 × 70 × 70 points, with grid point spacing of 0.375 Å. The Lamarckian Genetic Algorithm (LGA) was used with the default settings, and 500 LGA docking runs were performed.

CORCEMA-ST Calculations. The underlying theory of CORCEMA-ST has been described previously (*13*, *14*), as have the details of executing the CORCEMA-ST protocol (*15*, *25*). The number of protons in UDP-Gal*p* **1** or UDP **2** and the protons of the amino acid residues within the UGM binding site, the number of protein protons that experience direct RF irradiation, and their identities were read into the program on the basis of the PDB coordinates of the UDP-Gal*p* **1**−UGM or UDP **2**−UGM complex generated from the AutoDock (*16*) protocol. To accelerate the computation of the matrix, spectral densities were calculated for only those proton pairs having a distance of ≤5 Å. In the calculations, UDP-Gal*p* **1** or UDP **2** and the 26 amino acid residues within the binding pocket were included. The parameters related to relaxation were set up as suggested in previous publications (*26*, *27*). The order parameter S^2 was set to 0.25 for the methyl group (*28*), while for methyl−X relaxation, S^2 was generally kept in the range of 0.85. For Tyr and Phe, a simple $\langle 1/r^6 \rangle$ average was used for the dipolar relaxation between the aromatic and other protons. On the basis of the experimental conditions, the concentration of ligand was 4 mM and the ligand:protein ratio was kept fixed at 100:1. k_{on} was set to 10^8. Since the dissociation constant (K_D) of the UDP-Gal*p* **1**−UGM complex was reported to be 40 μM (*29*, 30), K_{eq} was set in the range of 10^4−10^6 and was modified further to obtain the best fit. The final value used in the calculation was 10^5. The correlation time (τ) was set in the ranges of 0.3−2.0 and 20−60 ns for the ligand in the free and bound states, respectively; after optimization, the final values were 0.3 and 50 ns, respectively. Since the protein signals at −1.0 ppm were irradiated for the STD experiment, we made the reasonable assumption that the methyl protons in Ile, Ala, Leu, and Val were instantaneously saturated, and that magnetization would take a finite time to spread to other protein and ligand protons (bound and free) through dipolar networks and chemical exchange. STD values were calculated as $\{[I_{0(k)} - I(t)_{(k)}]/I_{0(k)}\} \times 100$, with $I_{0(k)}$ being the intensity of the signal of proton k without saturation transfer at time zero and $I(t)_{(k)}$ being the intensity of proton k after saturation transfer during the saturation time t. For the comparison to the experimental STD values, an NOE R-factor is defined as (*13*)

$$R\text{-factor} = \sqrt{\frac{\sum (S_{\text{expt},k} - S_{\text{calc},k})^2}{\sum (S_{\text{expt},k})^2}}$$

In these equations, $S_{\text{expt},k}$ and $S_{\text{calc},k}$ refer to experimental and calculated STD values for proton k, respectively.

RESULTS

*Epitope Mapping of UDP-Gal*p* **1** and UDP **2** in the UGM Binding Site.* One-dimensional STD-NMR spectra for UDP-Gal*p* **1** and UDP **2** in the presence of UGM in the oxidized state are shown in Figure 1. Significant STD effects were observed in the spectra collected with and without spin-lock. The largest STD effect was observed for the protons of the uridine moiety, H1R/H5U, in UDP-Gal*p* **1** and UDP **2**. Thus, the STD intensity of this peak was set to 100% as a reference. The relative STD intensities for other protons were calculated on the basis of this peak intensity, as summarized in Figure 2.

All protons in UDP **2** exhibited strong STD signals, suggesting that it is in close contact with the protein protons in the UGM active site. Similar profiles were observed in the STD-NMR spectra of UDP-Gal*p* **1**, although the STD intensities from UDP-Gal*p* **1** were weaker. For the galactose moiety in UDP-Gal*p* **1**, significant STD effects were observed for the H1G, H4G, and H6G protons, although the intensities were relatively weak compared with those from

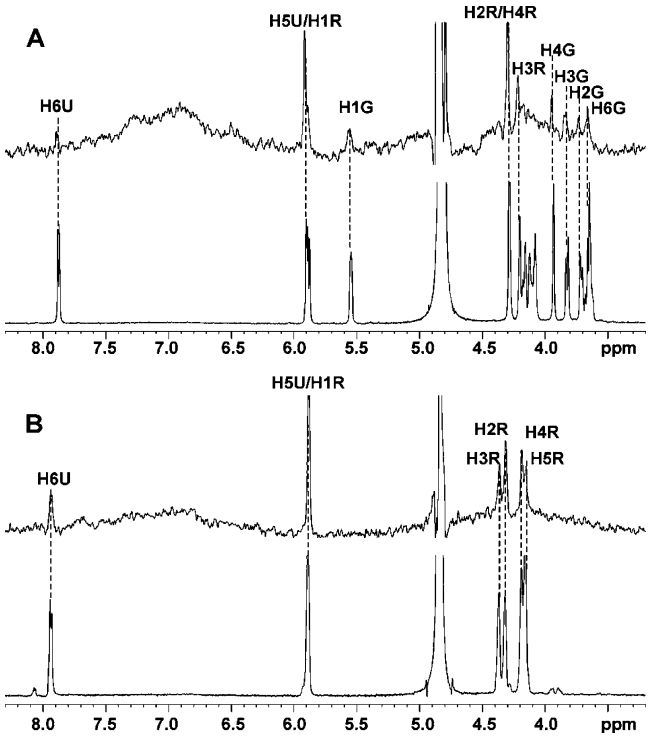

FIGURE 1: Expansions of the one-dimensional ^{1}H NMR spectra of (A) UDP-Gal*p* **1** and (B) UDP **2** at 600 MHz and 285 K in the presence of UGM. The reference (bottom) and the STD-NMR spectra (top) for each compound, recorded without water suppression, are shown (U for uracil, R for ribose, and G for galactopyranose).

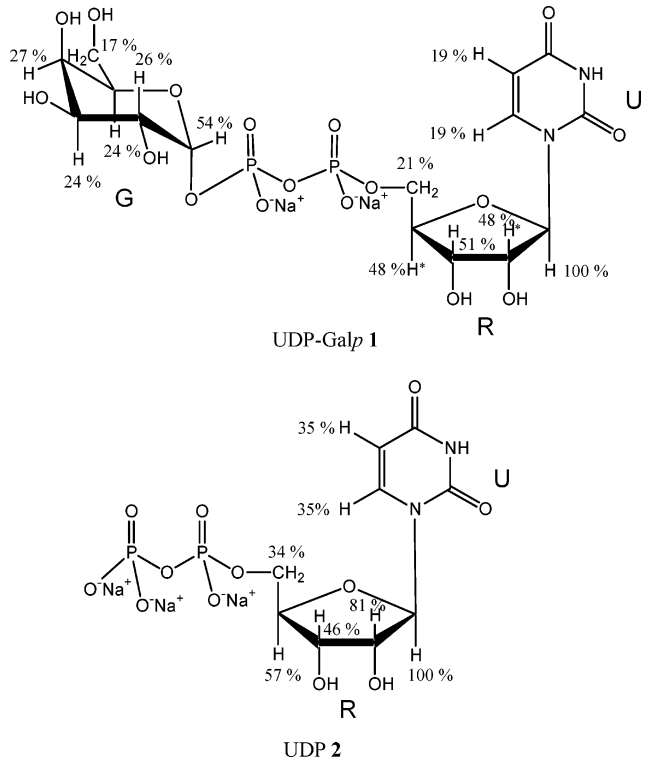

FIGURE 2: Epitope mapping of UDP-Gal*p* **1** and UDP **2** in the UGM binding site (U for uracil, R for ribose, and G for galactopyranose). The percentages reflect STD intensities relative to H1R (100%). The STD intensity for H2R and/or H4R was obtained from the overlapping peak at 4.28 ppm. The STD intensity of H5U was estimated and set to the same value as that of H6U based on calculation by the CORCEMA-ST protocol and the STD-NMR experiments for the UMP−UGM complex (see Figure 1 of the Supporting Information).

the uridine moiety. For other protons in this group (H2G, H3G, and H5G), the STD signals were weak. This result was reinforced by another STD experiment with Gal*p* 1-phosphate **3**, under identical conditions, in which extremely weak STD effects were observed (data not shown).

Competitive Binding of UDP-Galp 1 and UDP 2. Competition studies were performed to determine if the two ligands, UDP-Gal*p* **1** and UDP **2**, bind at or near the same site in UGM. STD-NMR titration experiments (*19*) were carried out at 285 K for the complexes of UGM with UDP-Gal*p* **1** and UDP **2** in different ratios. Figure 3 shows that when UDP-Gal*p* **1** was added to the UDP **2**−UGM complex in a 1:1 ratio, no STD NMR signals were observed from UDP-Gal*p* **1** (Figure 3C) until a ratio of 2:1 was reached (Figure 3D). Furthermore, STD signals from UDP-Gal*p* **1** were clearly seen at a UDP-Gal*p* **1**:UDP **2** ratio of 5:1 (Figure 3E). In contrast, UDP **2** yielded intense STD-NMR signals, and the signal intensity did not change significantly upon addition of UDP-Gal*p* **1** (Figure 3C−E), clearly indicating that UDP **2** is the higher-affinity ligand for binding to UGM in the oxidized state. STD-NMR titration experiments were also repeated after UDP **2** was added to the UDP-Gal*p* **1**−UGM complex in different ratios (data not shown). The magnitudes of STD signals for UDP-Gal*p* **1** were reduced dramatically at a UDP-Gal*p* **1**:UDP **2** ratio of 1:0.2, and then disappeared at a ratio of 1:0.5, supporting the previous conclusion.

Effect of Flavin Reduction on Ligand Binding. Previous studies of UGM have indicated that the enzyme is active only when flavin is reduced (*8*). STD-NMR experiments were therefore carried out for the complex of UDP-Gal*p* **1**, UDP **2**, and Gal*p* 1-phosphate **3** with UGM in the absence and presence of sodium dithionite. Significant STD signals were detected for UDP-Gal*p* **1** and UDP **2** under both these experimental conditions, suggesting that these two ligands can bind to UGM even when the enzyme is in its oxidized state. Upon addition of dithionite to the NMR sample, the color of the sample changed from yellow to colorless, suggesting that the FAD in UGM had been reduced (*9*). One-dimensional STD-NMR experiments were carried out immediately after addition of dithionite, and each experiment of 128 scans took 15 min. Experiments were continued for 24 h. However, no significant change in STD signal intensities was detected over this period of time. For the complex of Gal*p* 1-phosphate **3** and UGM, STD signals were still very weak, even in the presence of dithionite, suggesting that the UDP moiety in UDP-Gal*p* **1** might play the dominant role in its binding to UGM.

Although no significant change with the addition of dithionite was observed from STD-NMR spectra for UDP-Gal*p* **1** (Figures 3A and 4A) and UDP **2** (Figures 3B and 4B) individually, the relative binding affinity of UDP-Gal*p* **1** and UDP **2** exhibited dramatic changes upon the reduction of UGM as shown in competitive titration experiments. STD-NMR experiments were performed for these two ligands in different ratios in the presence of reduced UGM (Figure 4). As shown in Figure 3, when UGM was in the oxidized state, the STD signals were mainly from UDP **2**. Upon addition of dithionite, STD signals from both ligands were observed, even with a UDP-Gal*p* **1**:UDP **2** ratio of 0.2:1 (Figure 4C). When UDP-Gal*p* **1** and UDP **2** were present at a ratio of

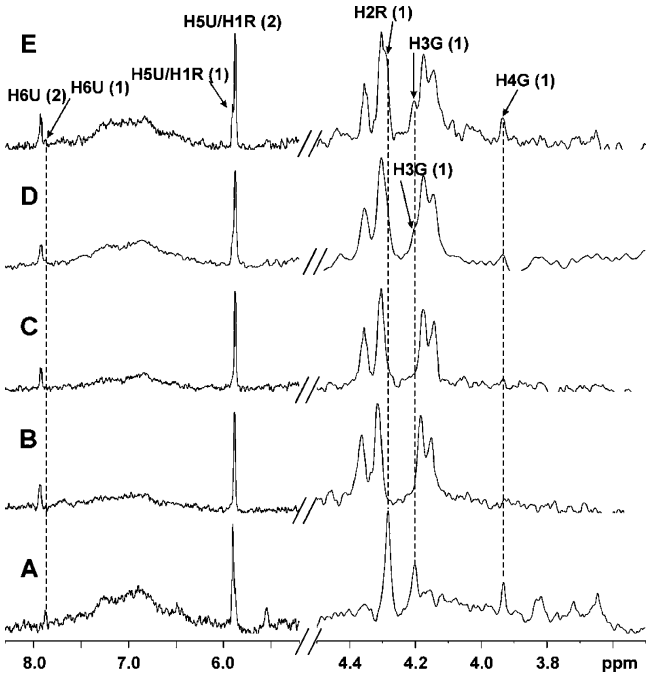

FIGURE 3: STD-NMR spectra for the competitive binding of UDP-Gal*p* **1** and UDP **2** to UGM in the oxidized state at 600 MHz and 285 K. (A) Low-affinity ligand UDP-Gal*p* **1** at a concentration of 4 mM in the presence of 20 μM UGM. (B) High-affinity ligand UDP **2** at a concentration of 4 mM in the presence of 20 μM UGM. (C) UDP-Gal*p* **1**:UDP **2** ratio of 1:1 showing that the STD signal intensities of UDP **2** were not affected significantly and no STD signals of UDP-Gal*p* **1** were detected. (D) UDP-Gal*p* **1**:UDP **2** ratio of 2:1 showing that very weak STD signals from UDP-Gal*p* **1** started appearing. (E) UDP-Gal*p* **1**:UDP **2** ratio of 5:1 showing the STD signals from UDP-Gal*p* **1** were observed (U for uracil, R for ribose, and G for galactopyranose).

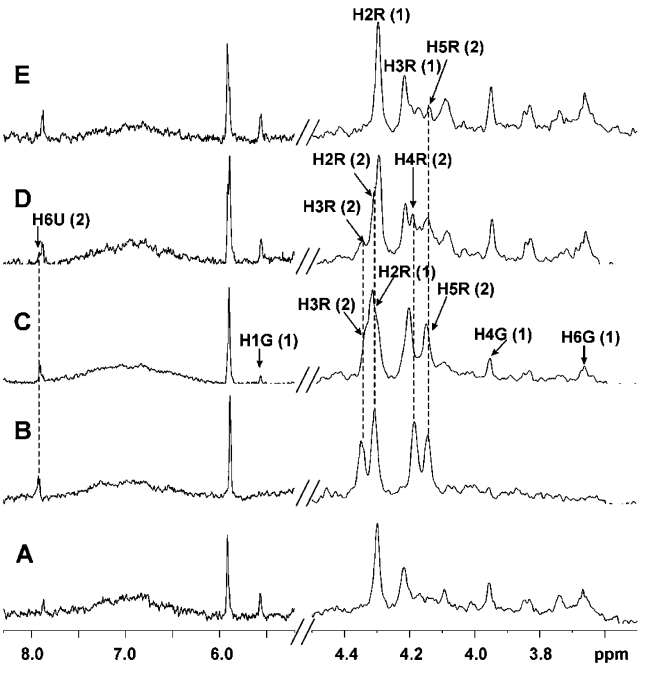

FIGURE 4: STD-NMR spectra for the competitive binding of UDP-Gal*p* **1** and UDP **2** to UGM in the reduced state at 600 MHz and 285 K. (A) UDP-Gal*p* **1** at a concentration of 4 mM in the presence of 20 μM UGM. (B) UDP **2** at a concentration of 4 mM in the presence of 20 μM UGM. (C) UDP-Gal*p* **1**:UDP **2** ratio of 0.2:1 showing that the STD signals from UDP-Gal*p* **1** were detected and the STD signal intensities of UDP **2** were not affected significantly. (D) UDP-Gal*p* **1**:UDP **2** ratio of 1:1 showing that significant STD signals from two ligands were observed and the signal intensities for UDP **2** were slightly weaker. (E) UDP-Gal*p* **1**:UDP **2** ratio of 2:1 showing STD signals were mainly from UDP-Gal*p* **1** and the STD signals from UDP **2** were still observable (U for uracil, R for ribose, and G for galactopyranose).

1:1, significant STD signals from both ligands were observed at the same time and the signals of UDP-Gal*p* **1** were slightly stronger (Figure 4D). When the UDP-Gal*p* **1**:UDP **2** ratio reached 2:1, STD signals were mainly from UDP-Gal*p* **1** but the STD signals from UDP **2** were still observable (Figure 4E). These results clearly show that the relative binding affinity of UDP-Gal*p* **1** increased upon the reduction of UGM.

Ligand Binding Mode in Monomer A of UGM. AutoDock (*16*) allows random movement of multiple ligand conformations on the protein surface. Therefore, it is possible to explore the potential binding pocket or the binding modes of ligands once the crystal structure of a protein is available. To obtain a viable binding mode for UDP-Gal*p* **1**, UDP **2** and Gal*p* 1-phosphate **3** were used as initial probe molecules to explore the putative active site of UGM; the information was intended to facilitate the subsequent docking of UDP-Gal*p* **1** in the active site.

For **2** and **3**, 300 docked structures, i.e., 300 runs, were generated by using the Lamarckian Genetic Algorithm searches and were clustered according to the results differing in positional root-mean-square deviation (rmsd). The lowest docked energy and the average energy of the cluster, together with the number of structures in each cluster, are listed in Table 1 of the Supporting Information, ranked in order of increasing energy. Of 25 clusters of binding modes of UDP **2**, the conformation with the lowest docked energy (−10.38 kcal/mol) gave the best match with the experimental data (Figure 5A). The *R*-factor calculated by CORCEMA-ST is 0.326, which suggests that the predicted binding mode correlates well with the results of the STD-NMR experiments (*15*). This lowest-energy docked structure of **2**, representing a likely binding mode (shown in Figure 6A), does dock in the putative active site of UGM, and interacts with Ala A55, Gln A155, Trp A156, Ile A167, Lys A169, Arg A278, Tyr A311, Asn A314, Tyr A346, and FAD.

In our study, several methods were used to assign the STD signals for H5U and H1R since the two peaks overlap. Several options for determining a value for H5U were available, for example, (a) calculating H5U/H1R as a pair and using the average STD intensity and (b) attributing the STD signal mainly to H1R, and giving a small value for H5U. We have carried out calculations with CORCEMA-ST with these different options for H5U/H1R. The test results showed that option b always gave a better fit with a lower *R*-factor. Information from the STD experiment for the complex of UMP and UGM also supports our assignment (see Figure 1 of the Supporting Information). In the spectra of the UMP−UGM complexes, H5U and H1R are separated well and both protons exhibit STD signals. However, the STD signal from H1R is strong and that from H5U weak, as inferred in the results shown in Figure 1 for the UDP **2**−UGM and UDP-Gal*p* **1**−UGM complexes. Our modeling data show that UMP exhibits a binding mode similar to that of UDP-Gal*p* **1** in the active site. For the STD intensities in the complex of UGM and UDP-Gal*p* **1**, we chose to use the

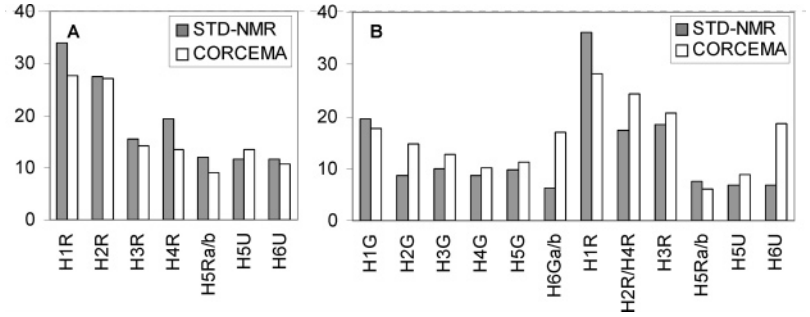

FIGURE 5: Comparison of experimental and predicted STD values from the CORCEMA-ST protocol for (A) UDP **2** and (B) UDP-Gal*p* **1** in the presence of UGM (U for uracil, R for ribose, and G for galactopyranose). Experimental STD values (gray bar) were calculated as $\{[I_{0(k)} - I(t)_{(k)}]/I_{0(k)}\} \times 100$, with $I_{0(k)}$ being the intensity of the signal of proton k without saturation transfer at time zero and $I(t)_{(k)}$ being the intensity of proton k after saturation transfer during the saturation time t. Theoretical STD values (white bars) are presented for the best fitting mode of UDP **2** and UDP-Gal*p* **1**, generated from the protocol combining AutoDock and CORCEMA-ST calculations. The calculations were performed using the following parameters: order parameter $S^2 = 0.85$, the concentration of ligand was 4 mM, the ligand:protein ratio was 100:1, $k_{on} = 10^8$, $K_D = 10$ μM, and $\tau = 0.3$ and 50 ns for the ligand in free and bound states, respectively.

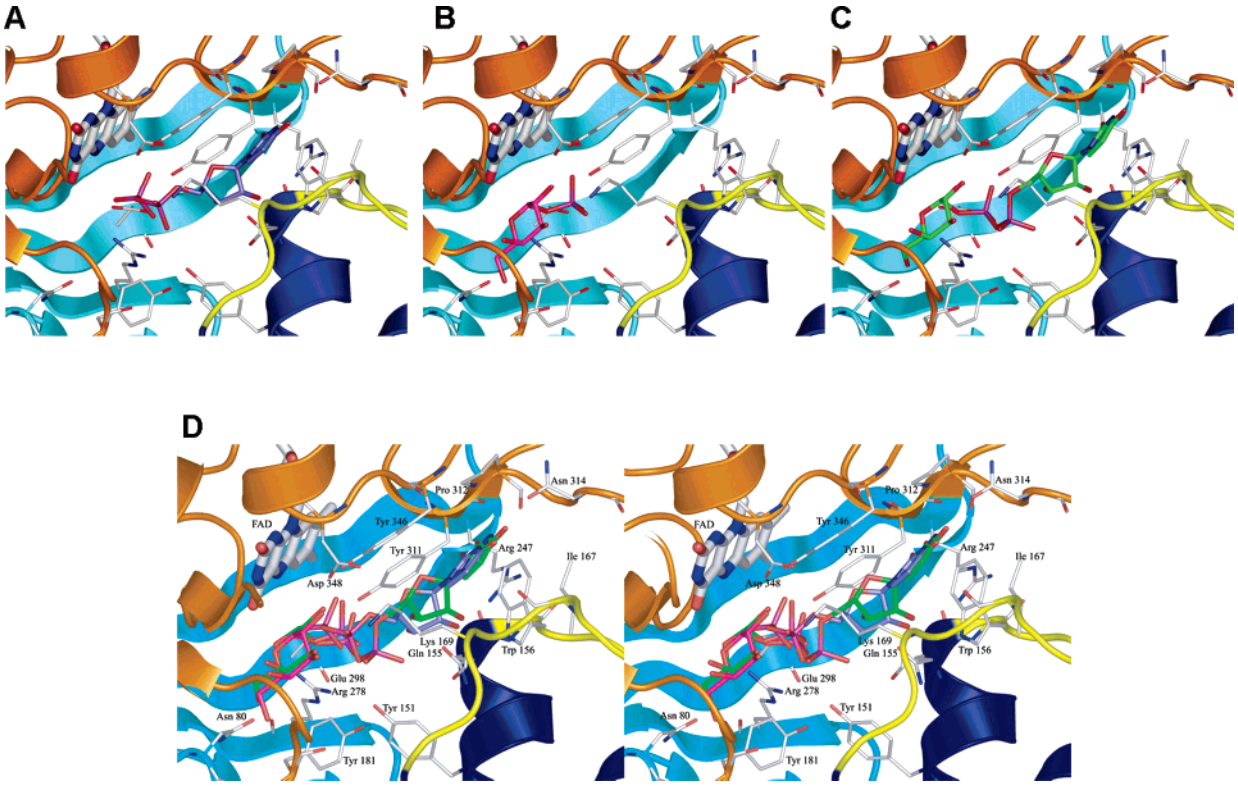

FIGURE 6: Binding modes observed for (A) UDP **2**, (B) Gal*p* 1-phosphate **3**, and (C) UDP-Gal*p* **1** in the putative active site of UGM from docking calculations. A stereoview of the superposition of **1** on **2** and **3** in the active site of UGM is shown in panel D. Domain 1 is colored orange, domain 2 blue, and domain 3 cyan. The two flexible loops are colored yellow. FAD, the relevant side chains, and compounds **1**−**3** are depicted as sticks (red for oxygen, blue for nitrogen, purple for phosphate, white for carbons of FAD and the relevant side chains, amethyst for carbon for UDP **2**, magenta for carbon for Gal*p* 1-phosphate **3**, and green for carbon for UDP-Gal*p* **1**).

same value for H5U and H6U since similar intensities for H5U and H6U were observed in the UMP−UGM STD spectra.

The lowest-energy docked structure of Gal*p* 1-phosphate **3**, representing a likely UGM−**3** complex structure, was also located in the putative active site of UGM, close to FAD, with a docked energy of −7.51 kcal/mol (Figure 6B). Ligand **3** is stabilized in the active site by interactions with residues Ala A55, Asn A80, Arg A278, Tyr A311, Tyr A346, and FAD.

The UGM−**2** and UGM−**3** complex structures thus obtained served as starting points for building an initial structure of UDP-Gal*p* **1**. Five hundred docked structures, i.e., 500 runs, were generated and ranked in 101 clusters, representing 101 binding modes, according to the results differing in positional root-mean-square deviation (2.0 Å). The lowest docked energy and the average energy of the first 25 clusters, together with the number of structures in each cluster, are listed in Table 1 of the Supporting Information, ranked in order of increasing energy. The dihedral angles of the conformations of UDP-Gal*p* **1** docked in the active site of UGM are listed in Table 2 of the Supporting Information.

On the basis of the final docked energies, the first 25 clusters of UDP-Gal*p* **1** were analyzed in light of information from previous mechanistic studies. The various possibilities were also evaluated by calculating the expected STD effects for a particular binding mode using the CORCEMA-ST

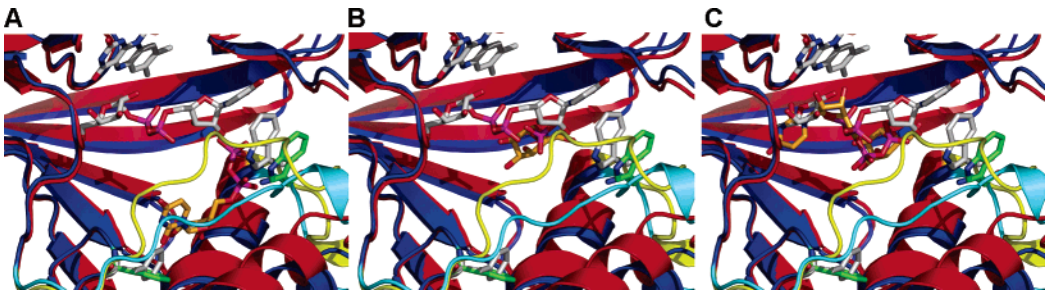

FIGURE 7: Comparisons of binding modes from docking calculations for (A) UDP **2**, (B) Gal*p* 1-phosphate **3**, and (C) UDP-Gal*p* **1** in monomer B with that of UDP-Gal*p* **1** in monomer A of UGM. Superposition of monomer A with monomer B is shown. Monomer A is colored red, with the mobile loop colored yellow, and monomer B is colored blue, with the loop colored cyan. FAD, the relevant side chains, and compounds **1**−**3** are depicted as sticks (red for oxygen, blue for nitrogen, purple for phosphate, gray for carbons of FAD, white for carbons in **1** in monomer A, and orange for carbons in **1**−**3** in monomer B). Trp 156 and Phe 95 are also shown (in gray for monomer A and in green for monomer B).

protocol, and then comparing these effects to the experimental results. Current mechanistic proposals for UGM indicated that the flavin isoalloxazine ring needs to be close to the anomeric position of the galactopyranose moiety to perform electron transfer (*8*, *9*) or form a covalent bond (*10*). Thus, according to the position of the galactopyranose ring of **1** in the active site, clusters 6, 9−11, and 13−25 were judged to be less likely because the distances (>4.5 Å) between N5 of the FAD and the C1 position of the galactopyranose moiety in **1** are too long for formation of a flavin−galactose interaction. In support of this conclusion, the CORCEMA-ST calculations for these conformers predicted very weak STD effects for most of the protons of UDP-Gal*p* **1**. Therefore, these binding modes can be discarded. The experimental STD-NMR results for the UDP-Gal*p* **1**−UGM complex were examined next, together with the theoretical STD values predicted by CORCEMA-ST for the remaining eight conformers. As shown by the STD spectra (Figure 1), significant differences were observed between the protons in the galactopyranose moiety and the ribose moiety. Only five clusters (1, 2, 4, 7, and 12) provided a good match with the experimental data, which showed stronger STD values for the protons in the ribose moiety than the galactopyranose moiety; consequently, these clusters exhibit low *R*-factors (Figure 5B). Besides unsatisfactory fitting to the experimental data, clusters 3, 5, and 8 could also be rejected because the uracil ring moiety was distant from Trp A156 that was presumed to form a stacking interaction with the uracil ring and was previously shown to be important for activity of UGM (*8*). A survey of the Protein Data Bank reveals that the uracil moiety in a ligand usually forms an interaction with an aromatic residue in parallel-displaced stacking arrangement or π-edge stacking arrangement (*31*). Our model indicates that the uracil moiety of UDP-Gal*p* **1** stacks against Trp A156 in a π-edge mode.

Therefore, on the basis of the combined analysis of experimental STD-NMR effects and the predicted effects from CORCEMA-ST calculations, cluster 1, with the lowest docked energy (−14.31 kcal/mol) and a low *R*-factor (0.482), was selected to represent the binding mode of UDP-Gal*p* **1** in monomer A, as shown in panels C and D of Figure 6. The interactions between UDP-Gal*p* **1** and the residues of UGM identified from the docking studies are summarized in Table 3 of the Supporting Information. It is worth noting that whereas the fits between the predicted and calculated STDs for the ribose moiety in UDP **2** (Figure 5A) are excellent, they appear to have be slightly worse for UDP-Gal*p* **1** (Figure 5B). A possible reason for this difference is the slightly different positioning of the ribose moiety in UDP **2** versus UDP-Gal*p* **1** within the active site (see Figure 6). We defer further optimization of UDP-Gal*p* **1** in the enzyme active site to a future study.

Role of the Flexible Loop in Substrate Binding. On the basis of the differences in the positioning of a flexible loop found in the crystal structures of UGM from *E. coli* (two conformations found, a "closed" conformation in monomer A and an "open" conformation in monomer B) and *K. pneumoniae* and *M. tuberculosis* (all found in an open conformation) (Figure 3 of the Supporting Information), we docked UDP-Gal*p* **1**, UDP **2**, and Gal*p* 1-phosphate **3** in the active site of monomer B to compare the effects of the position of the loop on substrate binding. The resulting binding modes are considerably different from those found with monomer A. All of the studies were carried out using the crystal structure of *E. coli* UGM as our model, and unless noted, all references refer to this structure (PDB entry 1I8T) (*8*).

The most favorable binding mode of UDP **2** in monomer B (see the orange structure in Figure 7A), with the lowest docked energy of −8.63 kcal/mol, is flipped in contrast to that in monomer A. In this case, the uracil ring of **2** is close to Phe B95, and the stacking interaction between Trp 156 and the uracil ring, observed in monomer A, is absent. Consequently, the arrangement of residues and their interactions with the bound UDP **2** in the active site are different from those seen in monomer A. Comparison of the UDP **2** structures in monomers A and B, upon superimposition of the two monomers, gave an rmsd of 8.11 Å. Moreover, no binding mode similar to that in monomer A was detected.

The lowest-energy docked structure of Gal*p* 1-phosphate **3** in monomer B, with a docked energy of −7.33 kcal/mol, representing a likely UGM−**3** complex structure, did dock in the putative active site of UGM, but was not in the vicinity of FAD (Figure 7B). It is stabilized in the active site by interactions with residues Tyr B151, Gln B155, Arg B247, Thr B277, Arg B278, Glu B298, and Tyr B311. We also found a binding mode that was similar to that in monomer A, but the docked energy for this structure was −6.64 kcal/mol; in contrast, that in monomer A was −7.51 kcal/mol.

Comparison of the binding modes of UDP-Gal*p* **1** in monomers A and B gave an rmsd of 5.59 Å, with the lowest docked energy in monomer B of −13.18 kcal/mol. In this mode (Figure 7C), the galactopyranose ring of **1** was not in

the proximity of the isoalloxazine ring of FAD. The uridine ring of **1** did not form a stacking interaction with Trp B156, but the interaction of the phosphate moiety of **1** with Arg B278 was observed, as also observed in monomer A. A binding mode that was similar to that in monomer A was also found, although it did not belong to the cluster with the lowest docked energy. The docked energy for this structure was −11.10 kcal/mol; in contrast, that in monomer A was −14.31 kcal/mol.

Theoretical STD effects were also calculated with CORCEMA-ST on the basis of the results from the docking study for monomer B. However, whether the binding mode of **1** was with the structure with the lowest docked energy or the structure similar to that in monomer A, the predicted STD effects for the uridine moiety in UDP-Gal*p* **1** were very weak, which do not match the experimental data (Figure 2 of the Supporting Information).

DISCUSSION

Direct Insights for Ligand Binding Provided by STD-NMR Experiments. STD-NMR studies, in conjunction with molecular modeling and CORCEMA-ST calculations of STD effects, described herein have demonstrated for the first time in solution how UDP-Gal*p* **1** is bound to UGM. Similar epitope mapping for UDP-Gal*p* **1** and UDP **2** was observed in the STD-NMR experiments, suggesting that these two ligands bind in the active site in similar orientations. In STD-NMR experiments, both UDP-Gal*p* **1** and UDP **2** exhibited significant signals, suggesting that the interactions between UGM with the uridine moieties in these two ligands might be critical for binding. As shown by the modeling study, the interactions are mainly from the stacking arrangement between the uracil ring and the conserved aromatic residues in the active site of UGM. In contrast, Gal*p* 1-phosphate **3** binds to the active site of UGM very weakly under identical experimental conditions. This result further indicates that the uridine moiety plays a dominant role in binding of UDP-Gal*p* **1** in the active site of UGM, which is useful information for the design of novel inhibitors.

It is true, however, that the interaction between UGM and the galactopyranose moiety in UDP-Gal*p* **1** is also important for its binding, especially in the (active) reduced state, as confirmed by the competitive STD-NMR experiments in this study. For the enzyme in the oxidized state, UDP **2**, as an inhibitor, has a higher binding affinity than the natural substrate, UDP-Gal*p* **1**. However, when UGM is active in its reduced state, the binding affinity of UDP-Gal*p* **1** is increased and is higher than (or comparable with) that of UDP **2**. We propose that this dramatic change might be attributed to the interaction between the galactopyranose moiety and the flavin isoalloxazine ring, as previously suggested (*8*) and corroborated by the modeling studies in this paper. In the reduced state of UGM, more favorable interactions between $FADH^-$ and the galactopyranose moiety in UDP-Gal*p* **1** are provided that, in turn, manifest themselves as stronger binding for this ligand in the enzyme active site.

Role of Loops Explored in the Docking Study. It is not surprising that the docking results for **1**−**3** in monomer B are different from those in monomer A. In the X-ray structure of UGM from *E. coli* (*8*), the loop consisting of residues 155−172 has *B*-factors as high as 31.74 and 43.93 $Å^2$ in monomers A and B, respectively, whereas the *B*-factors for highly ordered regions are around 24 $Å^2$, which suggests that the loop is highly flexible. Although the two monomers of UGM can be superimposed with a Cα rmsd of 1.46 Å for all 367 Cα atoms, the flexible loop is found in two different conformations, a closed conformation in monomer A and an open conformation in monomer B. The straight-line distance traveled from the Cα atom of A168 in monomer A to that in B is approximately 7 Å (see Figure 3 of the Supporting Information). The same loop in the UGM structures of *K. pneumoniae* and *M. tuberculosis* is opened even further, with an additional movement of approximately 4 Å (Figure 3 of the Supporting Information). This loop, together with three other loops, flanks the binding cleft in monomers A and B. Therefore, the shape of the binding cleft of monomer A is different from that of monomer B because of the movement of the loop.

On the basis of the results from the docking studies and STD-NMR spectroscopy, a hypothesis could be put forward with respect to the function of the mobile loop: the flexible loop might act as a gateway for substrate binding. The outcome of this loop movement is an apparent closure of the surface edge of the cleft, as seen in monomer A, to facilitate the reaction, and an opening of the surface edge of the cleft, as seen in monomer B, to allow access of the substrate to the active site. Our rationale is based on the following arguments.

First, the most favorable binding modes of **1** and **2** in monomer A have the lowest docked energies of −14.31 and −10.38 kcal/mol, respectively. These energies are lower than those in monomer B (−13.18 and −8.63 kcal/mol, respectively). Second, the mode of binding of **1** in monomer A from docking studies could explain the two flavin-dependent mechanisms for UGM [electron transfer mechanism (*9*) and covalent bond formation mechanism (*10*)], but that in monomer B could not. In both mechanisms, the galactopyranose ring of **1** should be close to the flavin isoalloxazine ring system, as shown in the binding mode obtained for monomer A; however, it is distant from the FAD in the binding mode in monomer B. Additionally, the spectroscopic evidence of the perturbation of the redox potential of flavin caused by the binding of UDP is consistent with the "closing" of the active site upon binding (*30*). Third**,** in monomer B, UDP-Gal*p* **1** and UDP **2** bound in different locations within the UGM active site (Figure 7A, C). The result is in conflict with the STD-NMR experimental data that suggest these two ligands exhibit similar binding epitopes and competitive binding, and that **1** and **2** should bind at or near the same site of UGM. Inconsistency was also shown in the results of the CORCEMA-ST calculations based on the predicted binding mode in monomer B (see Figure 1 of the Supporting Information).

Presumably, the mobile loop is in a closed conformation, as seen in monomer A, to facilitate the reactions between the FAD and the substrate. If this mobile loop is open, as seen in monomer B and the UGM structures of *K. pneumoniae* and *M. tuberculosis*, intermolecular binding of **1**−**3** with UGM might not be as favorable. The structure of the binding cleft in monomer A might be a closer approximation of the substrate-bound active site.

Binding Mode Inferred from the Combined STD-NMR and Modeling Protocol. Excellent correlation between STD-NMR

experiments and theoretical prediction by CORCEMA-ST was obtained for the binding modes of UDP-Gal*p* **1** and UDP **2**, thus validating the model for the UGM−UDP-Gal*p* **1** complex. In this mode, the bound UDP-Gal*p* **1** makes a total of 21 interactions with UGM, as summarized in Table 3 of the Supporting Information. All of the contacts between UDP-Gal*p* **1** and UGM involving amino acid side chains are made with absolutely conserved residues, except the contact to Asn 80, which is also found as a histidine. Tyr 311 and Tyr 346 were previously shown to be important for activity (*8*); however, roles for two other conserved tyrosines (Tyr 151 and Tyr 181) cannot be predicted from our model. The uracil ring of **1** forms a stacking interaction with Trp 156. The binding of the phosphate moiety of **1** to Arg 278 was also observed, but no interaction of Arg 247 and the phosphate group was found. This is consistent with the sequences of the recently reported eukaryotic UGM homologues, which do not have an Arg in this position (*32*). The galactopyranose ring of **1** was positioned close in space to the isoalloxazine ring of the FAD on binding, and the distance between N5 of FAD and the anomeric position of the galactopyranose C1 atom was 3.01 Å. This close contact is believed to be the structural foundation for the mechanism of UGM, which is consistent with previous studies (*8*−*10*). In this mode, the uridine moiety is surrounded by 15 residues within 3 Å of the active site in UGM. The galactopyranose moiety is located adjacent to the flavin isoalloxazine ring and faces a large cavity in the active site. Thus, the uridine moiety should exhibit greater STD effects from the saturated protein residues nearby, as indicated in the STD-NMR experiments.

The prediction for the binding model described here is based on the crystal structure of UGM in the oxidized state. Recently, the crystal structure of UGM from *K. pneumoniae* in its reduced state was reported and indicated no significant change for the active site of UGM upon the reduction of FAD (*9*). In our STD-NMR experiments, the same STD profiles were obtained for UDP-Gal*p* **1** and UDP **2** in the complex with the oxidized and reduced UGM, suggesting no significant change in the binding patterns upon the reduction of UGM. The interactions between the galactopyranose ring and the flavin isoalloxazine ring suggested by modeling are also confirmed in the reduced state of UGM, as also shown clearly by competitive STD-NMR experiments. Thus, the binding mode obtained for UGM in the oxidized state also provides insight into the binding of UDP-Gal*p* **1** to UGM in the reduced state.

In summary, STD-NMR experiments have provided direct information which shows that UDP-Gal*p* **1** exhibits different binding affinities for UGM in its oxidized and reduced states. Excellent correlation between experimental STD-NMR effects and those predicted by CORCEMA-ST suggested that the structure of the binding cleft in monomer A might be a good approximation of the substrate-bound active site, such correlation not being observed for the substrate complexes with monomer B. Docking studies within the active site of the two monomers in UGM lead us to propose that the mobile loop might act as a gateway for substrate binding. The predicted model for the UDP-Gal*p* **1**−UGM complex precedes one obtained by X-ray crystallography; the latter result when available will serve as a test of the rigor of our combined STD-NMR and molecular modeling protocol for the structural prediction of protein−ligand complexes.

ACKNOWLEDGMENT

We are grateful to Dr. N. R. Krishna for providing the CORCEMA-ST program and to Dr. Blair D. Johnston for helpful discussion.

SUPPORTING INFORMATION AVAILABLE

One-dimensional ^{1}H STD-NMR spectra of UMP in the presence of UGM (Figure 1), comparison of experimental and predicted STD values for the UGM−UDP **2** and UGM−UDP-Gal*p* **1** complexes based on the docking studies for monomer B (Figure 2), superposition of monomers A and B of UGM from *E. coli* and UGM from *K. pneumoniae* (Figure 3), calculated energies of UDP-Gal*p* **1**, UDP **2**, and Gal*p* 1-phosphate **3** docked in the active site of UGM (Table 1), dihedral angles of the conformations of UDP-Gal*p* **1** docked in the active site of UGM (Table 2), and interactions of polar groups of the bound model of UDP-Gal*p* **1** with residues in the active site of UGM (Table 3). This material is available free of charge via the Internet at http://pubs.acs.org.

REFERENCES

1. Brennan, P. J., and Nikaido, H. (1995) The envelope of mycobacteria, *Annu. Rev. Biochem. 64*, 29−63.
2. de Lederkremer, R. M., and Bertello, L. E. (2001) Glycoinositolphospholipids, free and as anchors of proteins, in *Trypanosoma cruzi*, *Curr. Pharm. Des. 7*, 1165−1179.
3. de Lederkremer, R. M., and Colli, W. (1995) Galactofuranose-containing glycoconjugates in Trypanosomatids, *Glycobiology 5*, 547−552.
4. de Arruda, M. V., Colli, W., and Zingales, B. (1989) Terminal β-D-galactofuranosyl epitopes recognized by antibodies that inhibit *Trypanosoma cruzi* internalization into mammalian cells, *Eur. J. Biochem. 182*, 413−421.
5. Stevenson, G., Neal, B., Liu, D., Hobbs, M., Packer, N. H., Batley, M., Redmond, J. W., Lindquist, L., and Reeves, P. (1994) Structure of the O-antigen of *Escherichia coli* K-12 and the sequence of its rfb gene-cluster, *J. Bacteriol. 176*, 4144−4156.
6. Nassau, P. M., Martin, S. L., Brown, R. E., Weston, A., Monsey, D., McNeil, M. R., and Duncan, K. (1996) Galactofuranose biosynthesis in *Escherichia coli* K-12: Identification and cloning of UDP-galactopyranose mutase, *J. Bacteriol. 178*, 1047−1052.
7. Pan, F., Jackson, M., Ma, Y. F., and McNeil, M. (2001) Cell wall core galactofuran synthesis is essential for growth of mycobacteria, *J. Bacteriol. 183*, 3991−3998.
8. Sanders, D. A. R., Staines, A. G., McMahon, S. A., McNeil, M. R., Whitfield, C., and Naismith, J. H. (2001) UDP-galactopyranose mutase has a novel structure and mechanism, *Nat. Struct. Biol. 8*, 858−863.
9. Beis, K., Srikannathasan, V., Liu, H., Fullerton, S. W. B., Bamford, V. A., Sanders, D. A. R., Whitfield, C., McNeil, M. R., and Naismith, J. H. (2005) Crystal structures of *Mycobacteria tuberculosis* and *Klebsiella pneumoniae* UDP-galactopyranose mutase in the oxidised state and *Klebsiella pneumoniae* UDP-galactopyranose mutase in the (active) reduced state, *J. Mol. Biol. 348*, 971−982.
10. Soltero-Higgin, M., Carlson, E. E., Gruber, T. D., and Kiessling, L. L. (2004) A unique catalytic mechanism for UDP-galactopyranose mutase, *Nat. Struct. Mol. Biol. 11*, 539−543.
11. Pongdee, R., and Liu, H. W. (2004) Elucidation of enzyme mechanisms using fluorinated substrate analogues, *Bioorg. Chem. 32*, 393−437.
12. Peng, J. W., Moore, J., and Abdul-Manan, N. (2004) NMR experiments for lead generation in drug discovery, *Prog. Nucl. Magn. Reson. Spectrosc. 44*, 225−256.
13. Jayalakshmi, V., and Krishna, N. R. (2002) Complete relaxation and conformational exchange matrix (CORCEMA) analysis of

intermolecular saturation transfer effects in reversibly forming ligand−receptor complexes, *J. Magn. Reson. 155*, 106−118.
14. Jayalakshmi, V., and Krishna, N. R. (2004) CORCEMA refinement of the bound ligand conformation within the protein binding pocket in reversibly forming weak complexes using STD-NMR intensities, *J. Magn. Reson. 168*, 36−45.
15. Jayalakshmi, V., Biet, T., Peters, T., and Krishna, N. R. (2004) Refinement of the conformation of UDP-galactose bound to galactosyltransferase using the STD NMR intensity-restrained CORCEMA optimization, *J. Am. Chem. Soc. 126*, 8610−8611; *127*, 7261.
16. Morris, G. M., Goodsell, D. S., Halliday, R. S., Huey, R., Hart, W. E., Belew, R. K., and Olson, A. J. (1998) Automated docking using a Lamarckian genetic algorithm and an empirical binding free energy function, *J. Comput. Chem. 19*, 1639−1662.
17. Wen, X., Yuan, Y., Kuntz, D. A., Rose, D. R., and Pinto, B. M. (2005) A combined STD-NMR/molecular modeling protocol for predicting the binding modes of the glycosidase inhibitors kifunensine and salacinol to Golgi α-mannosidase II, *Biochemistry 44*, 6729−6737.
18. Johnson, M. A., and Pinto, B. M. (2002) Saturation transfer difference 1D-TOCSY experiments to map the topography of oligosaccharides recognized by a monoclonal antibody directed against the cell-wall polysaccharide of Group A *Streptococcus*, *J. Am. Chem. Soc. 124*, 15368−15374.
19. Mayer, M., and Meyer, B. (2001) Group epitope mapping by saturation transfer difference NMR to identify segments of a ligand in direct contact with a protein receptor, *J. Am. Chem. Soc. 123*, 6108−6117.
20. Johnson, M. A., and Pinto, B. M. (2004) Saturation-transfer difference NMR studies for the epitope mapping of a carbohydrate-mimetic peptide recognized by an anti-carbohydrate antibody, *Bioorg. Med. Chem. 12*, 295−300.
21. Clark, M., Cramer, R. D., and Vanopdenbosch, N. (1989) Validation of the general-purpose Tripos 5.2 Force Field, *J. Comput. Chem. 10*, 982−1012.
22. Gasteiger, J., and Marsili, M. (1980) Iterative partial equalization of orbital electronegativity: A rapid access to atomic charges, *Tetrahedron 36*, 3219−3228.
23. Gasteiger, J., and Marsili, M. (1981) Prediction of proton magnetic resonance shifts: The dependence on hydrogen charges obtained by iterative partial equalization of orbital electronegativity, *Org. Magn. Reson. 15*, 353−360.
24. Cornell, W. D., Cieplak, P., Bayly, C. I., Gould, I. R., Merz, K. M., Ferguson, D. M., Spellmeyer, D. C., Fox, T., Caldwell, J. W., and Kollman, P. A. (1995) A second generation force field for the simulation of proteins, nucleic-acids, and organic molecules, *J. Am. Chem. Soc. 117*, 5179−5197.
25. Bhunia, A., Jayalakshmi, V., Benie, A. J., Schuster, O., Kelm, S., Krishna, N. R., and Peters, T. (2004) Saturation transfer difference NMR and computational modeling of a sialoadhesin-sialyl lactose complex, *Carbohydr. Res. 339*, 259−267.
26. Lipari, G., and Szabo, A. (1982) Model-free approach to the interpretation of nuclear magnetic resonance relaxation in macromolecules. 1. Theory and range of validity, *J. Am. Chem. Soc. 104*, 4546−4559.
27. Lipari, G., and Szabo, A. (1982) Model-free approach to the interpretation of nuclear magnetic resonance relaxation in macromolecules. 2. Analysis of experimental results, *J. Am. Chem. Soc. 104*, 4559−4570.
28. Dellwo, M. J., and Wand, A. J. (1993) The influence of methyl rotor dynamics on hydrogen relaxation networks: Derivation of spectral densities in model-free form, *J. Am. Chem. Soc. 115*, 1886−1893.
29. Soltero-Higgin, M., Carlson, E. E., Phillips, J. H., and Kiessling, L. L. (2004) Identification of inhibitors for UDP-galactopyranose mutase, *J. Am. Chem. Soc. 126*, 10532−10533.
30. Fullerton, S. W. B., Daff, S., Sanders, D. A. R., Ingledew, W. J., Whitfield, C., Chapman, S. K., and Naismith, J. H. (2003) Potentiometric analysis of UDP-galactopyranose mutase: Stabilization of the flavosemiquinone by substrate, *Biochemistry 42*, 2104−2109.
31. Meyer, E. A., Castellano, R. K., and Diederich, F. (2003) Interactions with aromatic rings in chemical and biological recognition, *Angew. Chem., Int. Ed. 42*, 1210−1250.
32. Beverley, S. M., Owens, K. L., Showalter, M., Griffith, C. L., Doering, T. L., Jones, V. C., and McNeil, M. R. (2005) Identification of eukaryotic UDP-galactopyranose mutase (UGM/GLF) in microbial and metazoal pathogens, *Eukaryotic Cell 4*, 1147−1154.

BI0513406